Symmetry-based model for the modulated phases of betaine calcium chloride dihydrate

C. Kappler and M. B. Walker
Department of Physics, University of Toronto, Toronto, Ontario M5S 1A7, Canada
(Received 31 March 1993)

A symmetry-based model for betaine calcium chloride dihydrate (BCCD) is presented. BCCD is a crystal with many modulated phases that can be commensurate or incommensurate. In our model, BCCD is viewed as formed of layers, perpendicular to which the crystal is modulated. The free energy is expanded in terms of amplitudes of symmetry modes of these layers. Which symmetry modes must appear in the free energy is determined through experimental data on the phonon-dispersion relation. For a previous related work, the phonon-dispersion relation was not yet available and the necessary assumption of which modes should be included proved to be incorrect. In the free energy, competing interactions between the symmetry modes lead to different phases. The phase sequence derived from this model corresponds fairly well to what is found in experiment, but incommensurate and higher-order commensurate phases are overemphasized. The polarity of the phases determined by the model agrees with experimental data.

I. INTRODUCTION

The crystal betaine calcium chloride dihydrate (BCCD) shows an exceptionally large number of modulated phases, which are commensurate or incommensurate with the underlying lattice. This paper presents a model for BCCD which describes the dispersion relation of the low-lying phonon modes in the normal phase and the phase sequence and phase symmetry of the modulated phases.

Previous studies of modulated crystals have used a number of different approaches.[1] The most basic of these approaches makes use of rigid-ion-type model potentials as a basis for lattice-dynamical calculations of the phonon-dispersion relation, including the identification of the soft mode (see, e.g., Ref. 2). However, such calculations have not yet been done for BCCD. In another class of simplified models, there is only one variable per unit cell, and only a small number of neighboring unit cells interact.[3] Competing interactions in such models result in phase diagrams with a large number of modulated phases. Such models have had success in accounting for the wave-vector sequence observed in a wide variety of materials, but have not been successful in describing situations in which different space-group symmetries are possible for each wave vector. Models of this type that have been adapted to BCCD include the axial next-nearest-neighbor Ising (ANNNI) model[4] and the discrete frustrated ϕ^4 (DIFFOUR) model.[5] Landau-type theories have also been successful in accouting for phase transitions to modulated phases. However, this appraoch becomes impractical in cases where a large number of commensurate phases must be accounted for, since a different "lock-in" term in the free energy is required to stabilize each phase.[6] This type of model, too, was adapted to BCCD.[7]

This article makes use of symmetry-determined layer variables, following an approach introduced for the A_2BX_4 modulated structures by Chen and Walker.[8] We visualize BCCD as being formed of layers, perpendicular to which the crystal is modulated. We analyze the symmetry of the layers and find their symmetry modes (Secs. II A and II B). The free energy is expanded in terms of amplitudes of these so-called "layer modes." We consider the free energy as a function of temperature only. Competing interactions between the layer modes lead to different phases at different temperatures. The symmetry of the soft mode in the experimental phonon-dispersion relation[9] allows us to determine which of the layer modes possible must appear in the free energy (Secs. II C and II D). From the expression for the free energy we obtain the theoretical dispersion relation and the phase diagram (Sec. III). Because the model is built upon a symmetry analysis of BCCD, it not only predicts the phase sequence but also the symmetry and thus a possible spontanous polarization of each phase.

The model presented here is an extension of earlier work.[10,11] For the earlier model it was necessary to make assumptions about the relevance of each layer mode for the free energy, because the experimental phonon-dispersion relation was unavailable. However, when the dispersion relation was published, it became evident that the original choice of layer modes was incorrect. This was also suggested from an interpretation of a detailed structural analysis for the fourfold phase of BCCD.[12,13] We here present a new model based on the correct modes.

II. DEVELOPMENT OF MODEL

A. Description of BCCD

BCCD is a transparent, insulating crystal. Above the temperature $T_c = 165$ K, at normal pressure and zero

electric field, it is in a normal unmodulated phase. As a function of temperature, pressure, and electric field, BCCD attains different commensurate and incommensurate phases (see, e.g., Refs. 14–21). The structural change responsible for the phase transitions is an internal distortion in the x-y plane, modulated along the z axis. The modulation of each phase is described by a wave vector $\mathbf{k} = \alpha \mathbf{c}^*$, where $\mathbf{c}^*$ is the reciprocal-lattice vector in the z direction. The wave number α decreases monotonically with decreasing temperature, following an incomplete devil's staircase:[22] α locks in at simple fractions n/m (commensurate phases) and either jumps between or continuously moves through nonsimple fractions and irrational numbers (incommensurate phases) until it reaches zero. The value $\alpha = 0$ corresponds to an unmodulated phase, having a lower symmetry than the normal phase. Figure 1 shows the function $\alpha(T)$, summarizing experimental data.[17,20] Commensurate phases are labeled by the value of n/m in $\mathbf{k} = (n/m)\mathbf{c}^*$, where n/m is an irreducible fraction.

The experimental phonon-dispersion relation[9] in Fig. 2 shows that a soft mode causes the normal to incommensurate phase transition: The lowest mode of the phonon spectrum along $\mathbf{k} = (0, 0, k_z)$ develops a minimum that approaches the $\omega = 0$ axis as the temperature is lowered towards the transition temperature. The symmetry of the soft mode determines the symmetry of the incommensurate phase. Moreover, we assume that this soft mode also determines the symmetry of all other modulated phases which appear when the temperature is lowered further. This assumption is verified experimentally for the $\frac{1}{4}$ phase.[13]

The possible space groups of the commensurate phases are shown in Table I. They were derived theoretically in Ref. 24. The space group of the phase n/m depends only on whether n and m are even or odd, and on the phase angle Φ of the modulation relative to the unit cell. Some space groups allow a spontanous polarization of the corresponding phase, explaining why an electric field affects BCCD's phase sequence.

B. Symmetry analysis of BCCD

The crystal structure of BCCD in the normal phase is orthorombic with space group $Pnma$. There are four structural units $[(CH_3)_3NCH_2COO{\cdot}CaCl_2{\cdot}2H_2O]$ per unit cell. The position of the individual ions is described in Ref. 25. We consider all ions in the unit cell as associated with one of the two planes at $z = c/4$ and $z = 3c/4$. For example, the four nitrogen ions in the unit cell are associated with these planes as shown in Fig. 3. Furthermore, the betaine unit $(CH_3)_3NCH_2COO$, containing a given nitrogen ion, is associated with the plane to which the nitrogen ion belongs. For the calcium ions and the $CaCl_2{\cdot}2H_2O$ units they are contained in, we proceed similarly. We call the set of ions associated with a given plane a "layer."

An arbitrary distortion of a layer is described as a linear combination of symmetry modes of this layer. The definition of a symmetry mode of wave vector $\mathbf{k}$ is that it must transform like a basis vector of an irreducible representation (IRREP) of the little group of $\mathbf{k}$. For a

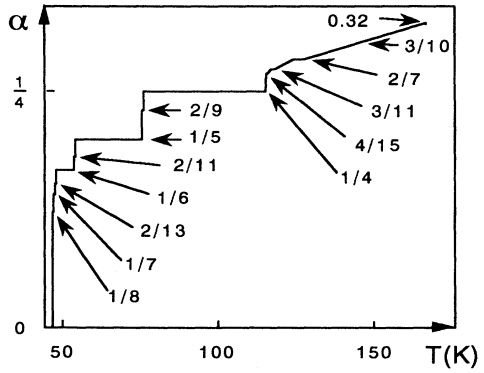

FIG. 1. Incomplete devil's staircase: the wave number $\alpha(T)$ for BCCD, labeling the phase sequence.

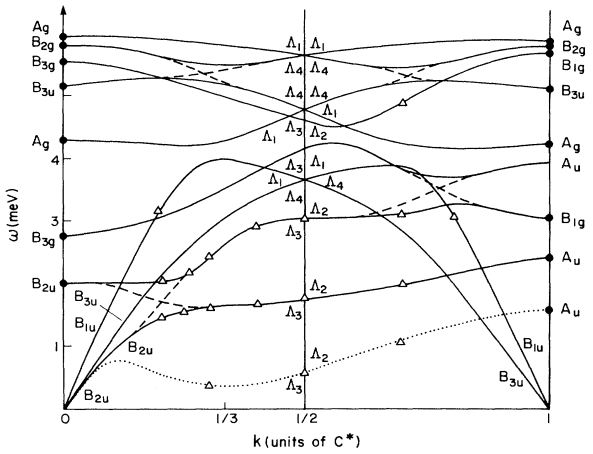

FIG. 2. Low-lying phonon branches in BCCD for $T = 270$ K (solid lines) and $T = 170$ K (dotted line), reprinted from Ref. 23. (△) and (•) indicate experimental data. (•) indicates experimental data, giving information over the symmetry of the mode as well.

TABLE I. Theoretically possible space groups of the commensurate phases (Ref. 24). $\alpha = n/m$ is the respective wave vector, Φ the phase angle of the modulation in the unit cell. **P** is the direction of a possible spontanous polarization. Boldy printed are the space groups realized according to experiments; note the ambiguity for n/m = odd/odd.

$\frac{n}{m}$	Label	Φ	Space group	**P**
	I	0	$P112_1/a$	
odd/odd	II	$\frac{\pi}{2}$	$P2_12_12_1$	
	III	arbitr.	$P112_1$	z
	I	0	$P2_1/n11$	
even/odd	II	$\frac{\pi}{2}$	**$Pn2_1a$**	y
	III	arbitr.	$Pn11$	y, z
	I	0	$P12_1/c1$	
odd/even	II	$\frac{n}{2m}\pi$	**$P2_1ca$**	x
	III	arbitr.	$P1c1$	x, z

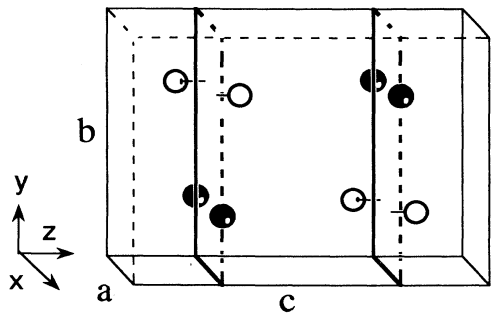

FIG. 3. Simplified unit cell of BCCD: (○) nitrogen ions, contained in betaine units; (●) calcium ions, contained in $CaCl{\cdot}2H_2O$ units.

symmetry mode of a layer, or "layer mode," $\mathbf{k}$ is two dimensional (2D). An arbitrary distortion of the crystal can be represented as a linear combination of layer modes from all layers. Therefore we can choose the layer modes as basic distortions of our model, without loss of generality.

The distortion of BCCD in the modulated phases is characterized by a wave vector $\mathbf{k} = (0, 0, k_z)$ normal to the layers (for convenience, the index z will be dropped when unambiguous). Therefore only layer modes with wave vector $\mathbf{k} = (0, 0)$, i.e., zone-center layer modes, will contribute to this distortion and for our purpose form a complete set of variables.

We now find the zone-center layer modes. Rather than work with the displacement of all ions in such a mode, we will, for the sake of simplicity, only work with the displacements of the nitrogen atoms. It is understood, however, that all ions in the layer have symmetry-determined displacements.

All zone-center layer modes (henceforth just called layer modes when unambiguous) must transform like basis vectors of the IRREP's of the little group of $\mathbf{k} = (0, 0)$. The wave vector $\mathbf{k}$ is invariant under the entire space group K of the layer, which therefore is its little group. It is easy to check (see Fig. 3) that the generators of K are $\{\sigma_z|\frac{1}{2}, 0\}$ and $\{\sigma_y|0, \frac{1}{2}\}$, and that its point group is C_{2v}. The character table and IRREP's Γ_i of C_{2v} are given in Table II. The characters of Γ_i define the transformation properties of the basis vector $e_l(\Gamma_i)$ of a layer mode of layer l. For Γ_2 and Γ_3 one finds the basis vectors (see Fig. 4)

$$e_l(\Gamma_2) = (0, 1, 0, 0, -1, 0), \quad e_l(\Gamma_3) = (0, 1, 0, 0, 1, 0), \tag{1}$$

TABLE II. Character table and irreducible representations of C_{2v}. The top row and the Γ_i refer to the 2D layer modes, the bottom row and the Λ_j to the 3D modes.

	E	C_{2x}	σ_y	σ_z	
Γ_1	1	1	1	1	Λ_1
Γ_2	1	1	−1	−1	Λ_2
Γ_3	1	−1	−1	1	Λ_3
Γ_4	1	−1	1	−1	Λ_4
	E	C_{2z}	σ_y	σ_x	

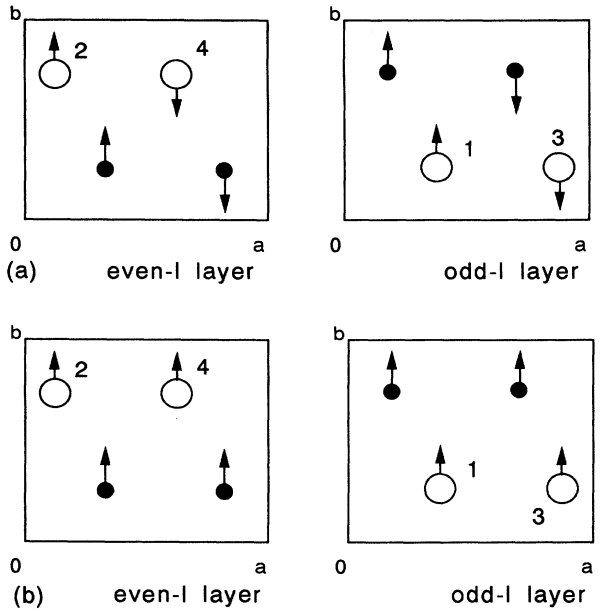

FIG. 4. Displacement of the nitrogen ions (○) and calcium ions (●) in a mode of (a) Γ_2 and (b) Γ_3 symmetry.

where the first three [last three] entries describe the displacement in the x, y, and z directions of the nitrogen ion number (1) [(3)] for odd l and of the nitrogen ion number (2) [(4)] for even l.

Note that the characters of the IRREP Γ_1 [Γ_4] allow two basis vectors $e(\Gamma_{1\alpha})$ and $e(\Gamma_{1\beta})$ [$e(\Gamma_{4\alpha})$ and $e(\Gamma_{4\beta})$], which we do not show in detail.

Now we use the symmetry of the soft mode (see Fig. 2) to identify those layer modes that form the modulated phases. The soft mode is a 3D symmetry mode. A given layer mode can only take part in forming the modulated phases if the 3D symmetry mode derived from it has the symmetry of the soft mode. It is easy to check that the superposition

$$e_k^i \equiv \sum_l \exp(ikz_l)\, e_l(\Gamma_i) \tag{2}$$

is a 3D symmetry mode with wave vector $\mathbf{k} = (0, 0, k)$. Here $z_l = l\tilde{c} + \tilde{c}/2$, $\tilde{c} = c/2$ is the interlayer distance, and the additional constant $\tilde{c}/2$ appears because the origin is chosen to be in the middle between two layers.

As symmetry modes, the e_k^i's must transform like basis vectors of an IRREP of the little group of $\mathbf{k} = (0, 0, k)$.

TABLE III. Irreducible representation of C_{2v} and D_{2h} according to which the basis vectors of the 3D symmetry modes e_k^i transform.

	$k = 0$	$0 < k < \frac{1}{2}c^*$	$\frac{1}{2}c^* < k < c^*$	$k = c^*$
$e_k^{1\alpha}$	B_{3u}	Λ_4	Λ_1	A_g
$e_k^{1\beta}$	A_g	Λ_1	Λ_4	B_{3u}
e_k^2	B_{3g}	Λ_3	Λ_2	A_u
e_k^3	B_{2u}	Λ_3	Λ_2	B_{1g}
$e_k^{4\alpha}$	B_{2g}	Λ_1	Λ_4	B_{1u}
$e_k^{4\beta}$	B_{1u}	Λ_4	Λ_1	B_{2g}

The generating elements of the group G, which leaves $\mathbf{k}$ invariant, are $\{\sigma_x|\frac{1}{2},\frac{1}{2},\frac{1}{2}\}$ and $\{\sigma_y|0,\frac{1}{2},0\}$. The point group is again C_{2v}. The corresponding IRREP's are labeled Λ_j (see Table II). In order to know according to which Λ_j the e_k^i transform, we need to know how the basis vectors $e_l(\Gamma_i)$ of the layer modes transform under the generatores of G. A look at Fig. 4 shows for example that

$$\{\sigma_x|\tfrac{1}{2},\tfrac{1}{2},\tfrac{1}{2}\}\, e_l(\Gamma_i) = e_{l+1}(\Gamma_i), \tag{3a}$$

$$\{\sigma_y|0,\tfrac{1}{2},0\}\, e_l(\Gamma_i) = -e_l(\Gamma_i), \qquad i=2,3; \tag{3b}$$

i.e., $e_l(\Gamma_2)$ and $e_l(\Gamma_3)$ transform identically. This allows us to derive the transformation properties of the 3D symmetry modes e_k^i, which are shown in the second and third columns of Table III. Because of Eq. (3), e_k^2 and e_k^3 transform identically, namely, like a basis vector of Λ_3 in the first half of the Brillouin zone and like a basis vector of Λ_2 in the second. As can be seen from Fig. 2, this is just how the soft mode transforms. On the other hand, $e_k^{1\alpha/\beta}$ and $e_k^{4\alpha/\beta}$ derived from Γ_1 and Γ_4 do not transform like basis vectors of the soft mode.

Finally, it will be useful to derive the symmetry of the 3D zone-center modes with $\mathbf{k}=(0,0,0)$ and its equivalent $(0,0,c^*)$, corresponding to $k=0$ and c^* in Eq. (2). The wave vector $\mathbf{k}=(0,0,0)$ is invariant under the full space group of the crystal, *Pnma*, which has generating elements $\{\sigma_x|\frac{1}{2},\frac{1}{2},\frac{1}{2}\}$, $\{\sigma_y|0,\frac{1}{2},0\}$, and $\{\sigma_z|\frac{1}{2},0,\frac{1}{2}\}$. Its point group is therefore D_{2h} with IRREP's A_p and B_{pi}, where the parity $p=u,g$ and $i=1,\ldots,3$.[26] To find how e_k^i transforms for $k=0$ and c^* under the action of *Pnma*, we need Eq. (3) and

$$\{\sigma_z|\tfrac{1}{2},0,\tfrac{1}{2}\}\, e_l(\Gamma_i) = \pm e_{-l}(\Gamma_i), \qquad i=2,3, \tag{4}$$

where the plus (minus) sign goes with Γ_3 (Γ_2). Note that here $e_l(\Gamma_2)$ and $e_l(\Gamma_3)$ transform differently. The resulting transformation properties of e_0^i and $e_{c^*}^i$ lead to the other columns in Table III.

The result of this section is that amplitudes of layer modes with basis vectors $e_l(\Gamma_2)$ and $e_l(\Gamma_3)$ must be included in the free energy, whereas those with $e_l^{\alpha/\beta}(\Gamma_1)$ and $e_l^{\alpha/\beta}(\Gamma_4)$ need not be.

C. Symmetry analysis of the experimental phonon-dispersion relation

For each layer, there are 168 distinct zone-center layer modes, because there are two structural units with 28 atoms each in the layer unit cell. Since the lowest-energy phonon branches are expected to be the most important for the description of the low-temperature phases, our model takes into account only a few low-lying branches which, according to the last section, must originate from layer modes with Γ_2 or Γ_3 symmetry. In particular, let us take into account three modes for each layer l as follows: one acoustic mode of Γ_3 symmetry and amplitude u_l, one optic mode of Γ_2 symmetry and amplitude v_l, and one optic mode of Γ_3 symmetry and amplitude w_l. Thus we consider the state of the crystal, and hence the free energy, to be determined by the amplitudes of u_l, v_l, and w_l of these three modes, the so-called "layer variables."

We expand the free energy in the harmonic approximation F_h to second order in powers of the layer variables and require it to be invariant under the operations of *Pnma* as well as an overall translation of the crystal, which is expressed as $u_l \to u_l + \delta$ (because u_l describes an acoustic mode). This expansion only considers the temperature dependence of the free energy. It yields

$$\begin{aligned} F_h = \sum_l [\, &\tfrac{1}{2}b_1\,(u_l-u_{l-1})^2 + \tfrac{1}{2}b_2\,v_l^2 + b_3\,v_l v_{l-1} + \tfrac{1}{2}b_4\,w_l^2 + b_5\,w_l w_{l-1} \\ &+ \tfrac{1}{2}b_6\,(u_l v_{l-1} - u_{l-1}v_l) + \tfrac{1}{2}b_7\,(2u_l - u_{l-1} - u_{l+1})w_l + \tfrac{1}{2}b_8\,(w_l v_{l-1} - w_{l-1}v_l)]. \end{aligned} \tag{5}$$

Note that none of the coefficients $\{b_i\}$ depends on l.

We now introduce the Fourier transforms

$$u_l \equiv i\sum_k e^{ikl\tilde{c}}\,u_k, \quad v_l \equiv \sum_k e^{ikl\tilde{c}}\,v_k, \quad w_l \equiv i\sum_k e^{ikl\tilde{c}} w_k, \tag{6}$$

which lead to

$$F_h = L\sum_k (u_k, v_k, w_k)^*\, \Omega^2(k) \begin{pmatrix} u_k \\ v_k \\ w_k \end{pmatrix}, \tag{7}$$

where L is the total number of layers, and $\Omega^2(k)$ is the symmetric 3×3 matrix

$$\Omega^2(k) = \begin{pmatrix} b_1\,(1-\cos k\tilde{c}) & -\tfrac{1}{2}b_6\,\sin k\tilde{c} & \tfrac{1}{2}b_7\,(1-\cos k\tilde{c}) \\ & \tfrac{1}{2}b_2 + b_3\cos k\tilde{c} & -\tfrac{1}{2}b_8\sin k\tilde{c} \\ & & \tfrac{1}{2}b_4 + b_5\cos k\tilde{c} \end{pmatrix}. \tag{8}$$

Since we have no basis for an estimate of the effective mass associated with each mode, we assume they are unity. Then the eigenvalues of the matrix $\Omega^2(k)$ are $\omega^2(k)$, where $\omega(k)$ is a 3D symmetry-mode frequency.

For the unperturbed case $b_6=b_7=b_8=0$, i.e., no interaction between modes, the matrix is already diagonal, leading to the dispersion relation in Fig. 5(a).

For $b_6, b_7, b_8 \neq 0$, the resulting dispersion relation typically looks like that depicted in Fig. 5(b). Its most conspicuous feature is that the branches do not cross.

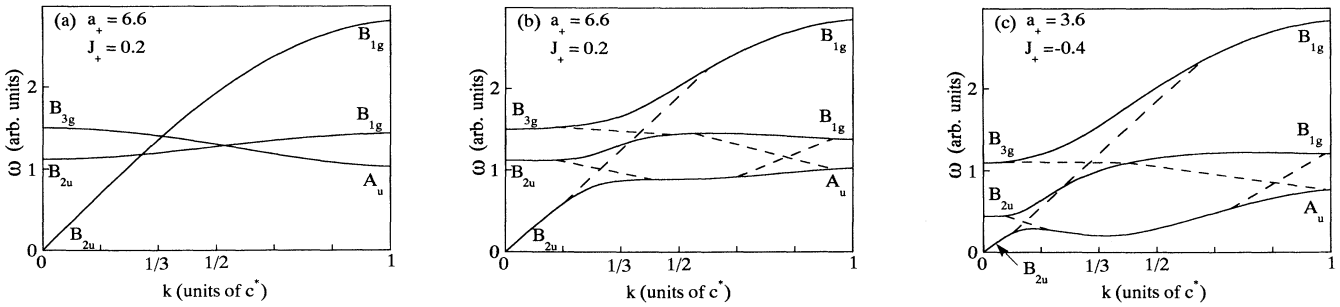

FIG. 5. The branches $\omega(k)$ of the theoretical dispersion relation, Eq. (8), with $b_2 - b_4 = 0$, $b_3 - b_5 = 1$, $b_1 = 4$. (a) No interaction between branches, i.e., $b_6 = b_7 = b_8 = 0$. (b) and (c) interaction "switched on," with $b_6 = -2$, $b_7 = 1$, $b_8 = 1$. Dashed lines indicate the course of the former unperturbed branches (crossovers). For a definition of a_+ and J_+ see Eq. (10).

Instead they—figuratively speaking—exchange their second halfs. It is easy to prove that along with this, there is an exchange of end-point symmetries: For example, in the no-interaction case [Fig. 5(a)], the acoustic branch starts with symmetry B_{2u} at $k = 0$ and ends with B_{1g} for $k = c^*$ as prescribed by Table II, whereas for nonzero interactions [Fig. 5(b)] the acoustic branch connects B_{2u} to A_u. Clearly, the A_u symmetry is picked up from the highest optic branch.

Now we apply these theoretical results to the experimental dispersion relation. According to Fig. 2, the soft mode is composed of two branches, both of which originate from Γ_3 layer modes, one acoustic and one optic. Following one branch along the dashed lines, i.e., the crossovers, one should retrieve the unperturbed branch. However, it is clear that the number of crossovers proposed in Fig. 2 is insufficient, because the zone-center symmetries do not fit. E.g., the lowest optic unperturbed branch should connect B_{2u} to B_{1g}. However, it ends on A_u. This means the crossovers must be different, in particular a Γ_2 branch; i.e., the optic branch which starts second lowest on the $k = 0$ axis must cross also, introducing the A_u zone-center symmetry.

Figure 5(b) shows the simplest way to satisfy both symmetries and the experimental data. Note that here the soft mode is composed of three rather than two unperturbed branches.

In the experimental dispersion relation four Λ_3/Λ_2 branches appear. The energetically highest of them is not considered in our model, because we assume it has no significant influence on the soft mode and thus on the phase transition. However, this branch seems to cross the second highest Λ_3/Λ_2 branch (the crossover is not indicated in Fig. 2) and therefore provides it with a different zone-center symmetry and shape from what is depicted in Fig. 5(b).

The result of this section is that a description of the dispersion of the soft mode requires the three layer modes with amplitudes u_l, v_l, w_l definded above. In the previous model[10] the free energy depended only on the two optic modes v_l and w_l.

D. Free energy for BCCD

Finally, we can present the full expression for the free energy, subject to the same conditions as the harmonic truncation F_h in Eq. (5). It is an expansion to fourth-order in w_l and v_l, but only to second order in u_l. The fourth-order terms involving u_l were dropped, because the coefficient for the quadratic term in u_l, b_1, can never become smaller than zero, for if it does, the velocity of sound in the crystal $v_s = \sqrt{b_1}$ becomes imaginary. However, only in the case $b_1 < 0$ are fourth-order terms involving u_l important. Interactions between layers are considered up to second order, within layers up to fourth order. This yields a free energy F given by

$$\begin{aligned} F = \sum_l [& \tfrac{1}{4} v_l^4 + \tfrac{1}{4} w_l^4 + \tfrac{1}{2} b_0 v_l^2 w_l^2 + 2 (u_l - u_{l-1})^2 \\ & + \tfrac{1}{2} b_2 v_l^2 + b_3 v_l v_{l-1} + \tfrac{1}{2} b_4 w_l^2 + b_5 w_l w_{l-1} \\ & + \tfrac{1}{2} b_6 (u_l v_{l-1} - u_{l-1} v_l) + \tfrac{1}{2} b_7 (2u_l - u_{l+1} - u_{l-1}) w_l \\ & + \tfrac{1}{2} (v_{l-1} w_l - v_l w_{l-1})]. \end{aligned} \tag{9}$$

Four coefficients are eliminated by rescaling, such that they are replaced by their respective value in Fig. 5(b). Seven coefficients $\{b_i\}$ are left. This large number is a consequence of having three interacting modes.

III. RESULTS

A. Theoretical dispersion relation

To get an estimate of the value and temperature dependence of the $\{b_i\}$, we fit the theoretical dispersion relation to the the softening of the lowest branch as found in experiment (Fig. 2, dotted line). The values of the $\{b_i\}$ are found by looking at details of Fig. 2. It turns out that one needs $b_3 > 0$ and $b_5 < 0$, but that the shape of the phonon branches is rather insensitive to the magnitude of the $\{b_i\}$. We define

$$a_\pm \equiv b_2 \pm b_4, \quad J_\pm \equiv b_3 \pm b_5, \tag{10}$$

and find that a softening of the lowest branch is achieved by lowering only a_+ and J_+, keeping a_-, J_- and all other coefficients fixed. This corresponds to a simultanous lowering of the unperturbed optic branches. Figure 5(c) shows the results of this simulation. The agreement with the experimental soft mode is excellent.

B. Theoretical phase diagram

1. Qualitative considerations

What mechanism leads to different phases when the coefficients $\{b_i\}$ are varied? Each phase, except for the nomal phase, is characterized by nonzero values of at least some of the layer variables u_l, v_l, w_l. In this section we only look at their signs. To mimimize F, each term in the free energy favors a different wave number, i.e., periodicity in l. For example, depending on the sign of its coefficient, a self-interaction term such as $v_l v_{l-1}$ will support either a ferroelectric $(----)$ or an antiferroelectric $(+-+-)$ profile for v_l. Other terms, such as the mixed interaction term $(v_{l-1}w_l - v_l w_{l-1})$, favor different profiles, in this case $(++--)$ for v_l and $(+--+)$ for w_l simultanously. Depending on the relative strength of the coefficients, the global minimum is located such that the resulting wave number is a trade-off between the different terms. As the size of the coefficients varies, the location of the minimum shifts, as does the wave number of the phase.

For BCCD, the sequence of wave numbers $\alpha(T)$ (see Fig. 1) is surprisingly well described by the so-called Farey tree,[16] a section of which is shown in Fig. 6. The Farey tree[27] is a 2D scheme for ordering the rational numbers between one and zero according to their size horizontally and to the size of the sum of their continued-fraction expansion vertically. The vertical rank is thus a measure of the simplicity or order of a number. Each number can be ascribed two "parents," namely, its two nearest neighbors from the upper rows. In fact, the numerator (denominator) of this number is obtained by adding the numerators (denominators) of its parents. In the phase sequence of BCCD, a phase n/m generally only appears if its parents appear as well and then always between them. In fact, such a phase sequence is predicted by most theoretical models, independent of the specific crystal they are dealing with.[3–5,8,10,22]

2. Quantitative results

Rather than determining a 7D phase diagram as a function of the seven $\{b_i\}$, we only consider a 2D cut

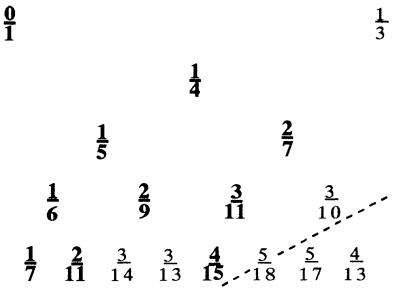

FIG. 6. Section of the Farey tree: a scheme for ordering the rational numbers between one and zero. Boldly printed are phases occuring in BCCD. Phases above the dashed line are included in the calculation of the phase diagram.

along a_+ and J_+, since changing these two quantities was sufficient to simulate the temperature dependence of the dispersion relation in the normal phase. The values of the other coefficients are those used to obtain Figs. 5(b) and 5(c). To minimize F, we simultanously solve the equations

$$
\begin{aligned}
0 &= \tfrac{\partial F}{\partial u_l} = 4\,(2u_l - u_{l-1} - u_{l+1}) + \tfrac{1}{2} b_6\,(v_{l-1} - v_{l+1}) \\
&\quad + \tfrac{1}{2} b_7\,(2w_l - w_{l-1} - w_{l+1}), \\
0 &= \tfrac{\partial F}{\partial v_l} = v_l^3 + b_0\, v_l w_l^2 \\
&\quad + \tfrac{1}{2}(a_+ + a_-)\, v_l + \tfrac{1}{2}(J_+ + J_-)(v_{l-1} + v_{l+1}) \\
&\quad + \tfrac{1}{2} b_6\,(u_{l+1} - u_{l-1}) + \tfrac{1}{2}\,(w_{l+1} - w_{l-1}), \\
0 &= \tfrac{\partial F}{\partial w_l} = w_l^3 + b_0\, v_l^2 w_l \\
&\quad + \tfrac{1}{2}(a_+ - a_-)\, w_l + \tfrac{1}{2}(J_+ - J_-)(w_{l-1} + w_{l+1}) \\
&\quad + \tfrac{1}{2} b_7\,(2u_l - u_{l-1} - u_{l+1}) \\
&\quad + \tfrac{1}{2}\,(v_{l-1} - v_{l+1}) \quad \forall\, l.
\end{aligned}
\tag{11}
$$

Because there are two layers per unit cell, a phase n/m has period $2m$ and $2n$ nodes. This leads to the boundary conditions $u_{l+2m} = u_l$, etc. One is left with $3 \times 2 \times m$ coupled nonlinear equations, to be solved numerically.

The phase diagram is traced out by noting that for $a_+ >> 0$ the normal phase, i.e., $u_l = v_l = w_l = 0$, is a solution, which therefore corresponds to high temperature, and consequently $a_+ << 0$ corresponds to low temperature. Given $a_+ << 0$, for $J_+ << 0$ the ferroelectric solution is stable, whereas for $J_+ >> 0$ the antiferroelectric solution is stable. This corresponds to $n/m = 0/1$ and $n/m = 1/0$, respectively.

The numerical procedure then consists of first guessing what phase n/m minimizes F for a given a_+ and J_+. For the same J_+ but $a_+ << 0$ this phase is still metastable. In fact, a phase with any wave number is metastable for $a_+ << 0$, because in this case all mixing terms in Eq. (11) are negligible and the solution can be any permutation on the layers of the analytical solutions $u_l = 0$, $\pm 2^{1/2}$, $v_l = 0$, $\pm|\tfrac{1}{2}(a_+ + a_-)|^{1/2}$, and $w_l = 0$, $\pm|\tfrac{1}{2}(a_+ - a_-)|^{1/2}$. For a phase n/m, the solution is a permutation of these values on $2m$ layers with $2n$ nodes. All permutations consistent with this number of nodes must be considered. Starting from one of these analytical solutions, one can proceed to higher values of a_+ in an iteration where the last solution is used as initial conditions for a new calculation with slightly increased a_+. For each pair (a_+, J_+), the free energy of different phases n/m is compared and the global minimum found. Once a rough phase diagram is determined, experience shows that one can choose further solutions according to the Farey tree. All phases listed in Fig. 6 above the dashed line were tested as well as all phases appearing in the logical extension of this scheme in the next lower row. In addition, we determine where high-order phases,

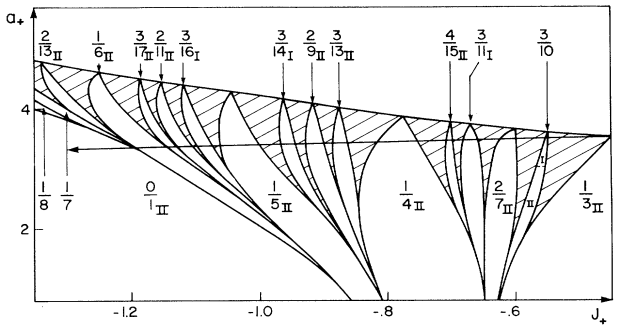

FIG. 7. Phase diagram for BCCD, obtained numerically from Eq. (9) with $b_6 = -2$ and $b_7 = 1$ as in Fig. 5, and $b_0 = 2$. Commensurate phases are labeled by n/m and their space group I–III from Table I. Shaded areas stand for high-order commensurate or incommensurate phases. The dashed line in phase $\frac{3}{10}$ marks a second-order phase transition in the space group. The bold arrow indicates the trajectory BCCD takes through the diagram at normal pressure.

including incommensurate phases, are stable by testing phases from two rows below the dashed line.

Note that the values of a_+ and J_+ at a normal$\rightarrow n/m$ phase transition are determined by the dispersion relation in Eq. (8), because for these values there must be a soft mode with $\omega(\frac{n}{m}c^*) = 0$.

The phase diagram obtained from solving Eqs. (11) is shown in Fig. 7. The qualitative features of the diagram are not sensitive to the magnitude of the coefficients $\{b_i\}$.

3. *Discussion*

The trajectory of BCCD on the phase diagram is a straight line, because we assume that the coefficients $\{b_i\}$ are linear functions of temperature. The trajectory is fixed on the one hand because the soft mode should touch the $\omega = 0$ axis at $\alpha = 0.32$.[15] On the other hand, $\frac{1}{8}$ is the last phase before finally entering the $\frac{0}{1}$ phase (see Fig. 1). We choose, however, to ignore the $\frac{1}{8}$ phase, because to our knowledge it was reported only once,[17] and was found through dielectric measurements; i.e., a small electric field was applied, whereas our model assumes zero electric field. At the same time including this phase would result in a very distorted theoretical phase sequence. Therefore the trajectory in Fig. 7 leads directly from $\frac{1}{7}$ to $\frac{0}{1}$.

However, even ignoring the $\frac{1}{8}$ phase does not completely eliminate the discrepancy between the theoretical and experimental phase sequences. Although all necessary phases appear in the theoretical sequence, many more phases of higher order appear between them. At the same time, the length of the trajectory in a given phase does not correspond well to the temperature intervall over which this phase is stable in experiment. Summarizing, the incommensurate and high-order commensurate phases take on more weight in the theoretical model than in experiment.

Since most experimental data originate from dielectric measurements, the agreement between theory and experiment might improve when the effect of an electric field is included in the expression for the free energy. Results from the previous model[11] suggest that doing so would indeed suppress high-order phases in favor of low-order phases.

The space groups of the phases predicted by our model all coincide with the space groups listed in Table I, and the polarity of the phases almost always agrees with the experimental results. Note that we find the space group $P2_12_12_1$ for the nonpolar odd/odd phases, for which no space group was determined experimentally.

For phases $n/m = \text{odd/even}$, we find the space group $P2_1ca$, if $m \leq 10$, and the space group $P12_1/c1$, if $m \geq 10$ (note the hybrid phase $\frac{3}{10}$). Therefore our model predicts that low-order odd/even phases can be spontanously polarized, whereas high-order phases of this type cannot. However, according to experiment odd/even phases are always spontanously polarized (see, e.g., Refs. 14 and 16–19).

The reason that the space group of odd/even phases depends on the order of the phase is the term $b_0 v_l^2 w_l^2$ in the expression for the free energy [see Eq. (9)]. For $b_0 = 0$ and n/m given, the nonpolar phase always has lower free energy than the polar phase. However, if $b_0 > 0$, $v_l = 0$ or $w_l = 0$ is supported, i.e., a profile in which the nodes of the modulation are located on layers. The location of the nodes is determined by the phase angle Φ of the modulation relative to the unit cell (see Table I). If, without loss of generality, we assume a sinusoidal modulation, then for $\Phi = n\pi/2m$, i.e., polar phase, the first and $(n+1)$st node are located on a layer, because the origin is in the middle between layers and because in a phase n/m the unit cell stretches over $2m$ layers. All other nodes are not located on a layer. For all other values of Φ in an odd/even phase, no node is located on a layer. Therefore, assuming similar magnitude of the layer variables in both phases, the polar phase is stable for b_0 sufficiently large. However, the effect of the b_0 term is the smaller the larger m, i.e., the order of the phase. Thus for m large, the nonpolar phase always prevails.

A comparison of the phase diagram derived here with that obtained from the previous model[10] shows that the two diagrams are essentially the same. Thus it is only in the interpretation of the dispersion relation that the need for a new model appears.

IV. SUMMARY AND OUTLOOK

In this paper a model was developed for BCCD, based on the introduction of appropriate symmetry-determined layer modes. The experimentally determined phonon-dispersion relation was used to identify the layer modes which are important to include in the formulation of the model. The model parameters were chosen such that the low-lying branches of the phonon-dispersion relation, including their temperature dependence, are well accounted for. The model then reproduces fairly well both the phase sequence and the phase symmetries found

in experiments. The main difference between theory and experiment is that high-order phases appear more prominently in the former. Tentatively, we concluded that the $\frac{1}{8}$ phase exists only in the presence of an electric field. To support this statement, future work will investigate the effect of an electric field on the theoretical phase diagram.

ACKNOWLEDGMENTS

M.B.W. would like to thank P. Nozières and the Theory College of the Institut Laue Langevin for their hospitality during a part of this work. This research was supported by the Natural Sciences and Engineering Research Council of Canada.

[1] *Incommensurate Phases in Dielectics*, edited by R. Blinc and A.P. Levanyuk (North-Holland, Amsterdam, 1986); H.Z. Cummins, Phys. Rep. **185**, 211 (1990).
[2] I. Etxebarria, J.M. Perez-Mato, and G. Madariaga, Phys. Rev. B **46**, 2764 (1992); H.M. Lu and J.R. Hardy, *ibid.* **42**, 8339 (1990), and references therein.
[3] W. Selke, in *Phase Transitions and Critical Phenomena*, edited by C. Domb and J.L. Lebowitz (Academic, New York, 1992), Vol. 15, p. 1.
[4] T. Tentrup and R. Siems, Ferroelectrics **105**, 379 (1990).
[5] T. Janssen, Z. Phys. B **86**, 277 (1992).
[6] J.C. Tolédano and P. Tolédano, *The Landau Theory of Phase Transitions* (World Scientific, Singapore, 1987).
[7] J.L. Ribeiro, J.C. Tolédano, M.R. Chaves, A. Almeida, H.E. Müser, J. Albers, and A. Klöpperpieper, Phys. Rev. B **41**, 2343 (1990).
[8] Z.Y. Chen and M.B. Walker, Phys. Rev. Lett. **65**, 1223 (1990).
[9] R. Currat, J.F. Legrand, S. Kamba, J. Petzelt, V. Dvořák, and J. Albers, Solid State Commun. **75**, 545 (1990).
[10] Z.Y. Chen and M.B. Walker, Phys. Rev. B **43**, 760 (1991).
[11] I. Folkins, M.B. Walker, and Z.Y. Chen, Phys. Rev. B **44**, 374 (1991).
[12] F.J. Zúñiga (private communication).
[13] J.M. Ezpeleta, F.J. Zúñiga, J.M. Pérez-Mato, W.A. Paciorek, and T. Breczewski, Acta Crystallogr. B **48**, 261 (1992).
[14] H.J. Rother, J. Albers, and A. Klöpperpieper, Ferroelectrics **54**, 107 (1984).
[15] W. Brill and K.H. Ehses, Jpn. J. Appl. Phys. **24**, Suppl. 24-2, 826 (1985).
[16] R. Ao, G. Schaak, M. Schmitt, and M. Zöller, Phys. Rev. Lett. **62**, 183 (1989).
[17] H.-G. Unruh, F. Hero, and V. Dvořák, Solid State Commun. **70**, 403 (1989).
[18] J.L. Ribeiro, M.R. Chaves, A. Almeida, J. Albers, A. Klöpperpieper, and H.E. Müser, J. Phys. Condens. Matter **1**, 8011 (1989).
[19] J.L. Ribeiro, M.R. Chaves, A. Almeida, H.E. Müser, J. Albers, and A. Klöpperpieper, Ferroelectrics **105**, 363 (1990).
[20] A. Almeida, M.R. Chaves, J.M. Kiat, J. Schneck, W. Schwarz, J.C. Tóledano, J.L. Ribeiro, A. Klöpperpieper, H.E. Müser, and J. Albers, Phys. Rev. B **45**, 9576 (1992).
[21] M.R. Chaves, A. Almeida, J.M. Kiat, W. Schwarz, J. Schneck, J.C. Tóledano, A. Klöpperpieper, H.E. Müser, and J. Albers, Phys. Rev. B **46**, 3098 (1992).
[22] P. Bak, Rep. Prog. Phys. **45**, 587 (1982).
[23] Reprinted from Ref. 9, copyright 1990, with the permission of Pergamon Press Ltd., Headington Hill Hall, Oxford OX3 0BW, UK.
[24] J.M. Perez-Mato, Solid State Commun. **67**, 1145 (1988).
[25] W. Brill, W. Schildkamp, and J. Spilker, Z. Kristallogr. **172**, 281 (1985).
[26] N. Hamermesh, *Group Theory* (Addison-Wesley, Reading, MA, 1962).
[27] G.H. Hardy and E.M. Wright, *An Introduction to the Theory of Numbers* (Oxford University, Oxford, 1979).